In vivo integrity of polymer-coated gold nanoparticles

Wolfgang G. Kreyling[1*], Abuelmagd M. Abdelmonem[2+], Zulqurnain Ali[2,3+], Alexander Wenk[1+], Frauke Alves[4,5+], Marianne Geiser[6+], Stephanie Hirn[1,7+], Raimo Hartmann[2+], Karsten Kantner[2+], Nadine Haberl[1,7+], Dorleta Jimenez de Aberasturi[2,8,9+], Gülnaz Khadem-Saba[1,10+], Jose-Maria Montenegro[2,11+], Joana Rejman[2+], Teofilo Rojo[8+], Idoia Ruiz de Larramendi[8+], Roser Ufartes[4+], Wolfgang J. Parak[2,9*]

[1] Institute of Lung Biology and Disease and Institute of Epidemiology 2, Helmholtz Zentrum München – German Research for Center for Environmental Health, 85764 Neuherberg / Munich, Germany

[2] Fachbereich Physik, Philipps Universität Marburg, Marburg, Germany

[3] present address: Department of Physics, Air University, Sector E-9, 44000 Islamabad, Pakistan

[4] Department of Molecular Biology of Neuronal Signals, Max-Planck-Institut für Experimentelle Medizin, 37075 Göttingen, Germany

[5] Department of Hematology and Oncology, University Medical Center Göttingen, Göttingen 37075, Germany

[6] Institute of Anatomy, University of Bern, 3012 Bern, Switzerland

[7] present address: Walter Brendel Centre of Experimental Medicine, Ludwig-Maximilians-University, 81377 Munich, Germany

[8] Department of Inorganic Chemistry, UPV/EHU, Bilbao, Spain

[9] CIC Biomagune, San Sebastian, Spain

[10] present address: Department of Chemistry, Industrial Biocatalysis, Technische Universität München (TUM), 85748 Garching, Germany

[11] present address: Central Research Services, University of Malaga, 29071 Málaga, Spain.

[+] authors listed in alphabetic order

[*] corresponding authors: kreyling@helmholtz-muenchen.de, wolfgang.parak@physik.uni-marburg.de

Keywords

colloidal nanoparticles, double radioactive labelling of NPs, *in vivo* biodistribution, intravenous injection, enzymatic degradation

Inorganic nanoparticles (NPs) are frequently engineered with an organic surface coating to improve their physicochemical properties, and it is well-known that their colloidal properties[1] may change upon internalization by cells[2, 3]. While the stability of such NPs is typically assayed in simple *in vitro* tests, their stability in a mammalian organism remains unknown. Here, we show that firmly grafted polymer shells around gold NPs may degrade when injected into rats. We synthesized monodisperse radioactively labelled gold nanoparticles (^{198}Au)[4] and engineered an ^{111}In-labelled polymer shell around them[5]. Upon intravenous injection into rats, quantitative biodistribution analyses performed independently for ^{198}Au and ^{111}In showed partial removal of the polymer shell *in vivo*. While ^{198}Au accumulates mostly in the liver, part of the ^{111}In shows a non-particulate biodistribution similar to intravenous injection of chelated ^{111}In. Further *in vitro* studies suggest that degradation of the polymer shell is caused by proteolytic enzymes in the liver. Our results show that even NPs with high colloidal stability can change their physico-chemical properties *in vivo*.

Upon internalization by cells, NPs are typically localized inside highly acidic endosomes and/or lysosomes. NPs are often stabilized by negatively charged groups (such as -COO^-) having pK_a values higher than the low pH values in the endosomes and lysosomes[6]. Thus, internalization leads to loss of charge and in consequence agglomeration[7]. Reduced pH also can enhance corrosion of NPs[8], resulting in release of toxic ions, as in the case of CdSe[9, 10] or Ag NPs[11, 12]. Besides changing the NP core properties, uptake by cells can also lead to a removal of their surface capping both *in vitro,* as shown for polymer-coated[3, 13] and dextrane-coated NPs[14], and *in vivo*[15, 16]. Intracellular enzymes may degrade the corona of adsorbed proteins[2], or may modify the surface chemistry of the NPs[17, 18]. To trace the fate of the different components of a NP – that is, the inorganic core, the organic surface capping, and the protein corona – each of these components needs to be labelled individually. Here, we labelled the core and shell of monodisperse Au NPs with radioisotopes[5] (Figure 1), and followed their respective biodistribution *in vivo*. Equal biokinetics of both radiolabels would indicate *in vivo* stability of the NPs, whereas different biodistributions would indicate partial degradation.

Au NPs with ^{198}Au label in their core and ^{111}In in their shell were intravenously injected into rats, which were sacrificed after 1 h or 24. Then complete organs of the rats were sampled and ^{198}Au and ^{111}In radioactivities originating from the different organs were measured[4, 19]. Blood contents of organs and the remaining body were calculated according to the findings of Oeff *et* al.[20]. In Figure 2a-d and Supplementary Fig. 25 the quantitatively balanced biodistributions (*i.e.* the sum of all ^{198}Au radioactivities and of all ^{111}In radioactivities as detected in all organs and tissues, the remaining carcass, and total faecal and urinary excretion is 100 %) are shown. For a detailed analysis of these data the stability of the radioactive labels needs to be known. The ^{198}Au within the stable ^{197}Au matrix resulting from the neutron-activation of the original gold NPs has been shown to dissolve negligibly out of the gold NPs cores, in particular after the washing procedure during the NP preparation[21]. Thus, the gold NPs are virtually insoluble[21] and therefore, their biokinetics is indicated by the ^{198}Au label.

By calculating the ^{111}In to ^{198}Au ratio for each organ and tissue and each time point, major differences between the retention of the two radio-isotopes become evident (Figure 2e, f). This differential behaviour indicates dissociation and removal of the ^{111}In label from the shell of the initial NP. Concerning the stability of the ^{111}In label in respect to its co-localization with the polymer shell, we have performed an auxiliary biokinetics studies in C57BL/6 mice. Hereby, a soluble form of the ^{111}In radio-isotope (as free ion) and of a complex of ^{111}In with the chelator diethylene triamine pentaacetic acid (DTPA) were intravenously injected, in order to distinguish the biodistribution of the soluble form (^{111}In ions) *versus* the chelated form (^{111}In-DTPA) and *versus* the particulate form (polymer coated Au NPs with ^{111}In in the polymer shell, *cf.* Figure 2c, d). By using the same quantitative approach as used for the data in Figure 2, data from Figure 3 allow for distinguishing whether ^{111}In has been released from the Au cores in the form of free ions (*i.e.* the shell label is lost) or in chelated form (*i.e.* as fragment from the polymer shell). In case of the ionic form ^{111}In is rapidly accumulated (time point 3 h) and retained (time point 24 h) in the liver (dark grey bars in Figure 3, Supplementary Fig. 29). However, in the case of the chelated form ^{111}In is efficiently excreted by urine (light grey bars in Figure 3).

Most of the ^{111}In as administered in particulate form is retained in the liver (*cf.* Figure 2c, d). Our data do not indicate whether the In in the liver is still attached to the polymer shell and thus the Au core, or is present in the form of free ions, as in both cases dominant retention in the liver

occurs (*cf.* Figure 2a, b and dark grey bars in Figure 3). On the other hand, the In excreted *via* urine is present in chelated form, as this is the only efficient pathway for renal excretion (*cf.* the light grey bars in Figure 3). Thus, in a likely scenario parts of the polymer shell (with the chelated In) come off the Au cores in the liver and these fragments are excreted by urine.

To probe where the polymer shell begins to separate from its Au core in the liver where most NPs are found, we performed histology (*cf.* Figure 2a-d). Au cores with chelated In in their shell (without using radioisotopes) were intravenously administered to rats with the same protocols used for the biodistribution studies shown in Figure 2. However, no Au NPs were detected in tissue slices of the liver when imaged with transmission electron microscopy (TEM) (*cf.* Supplementary Fig. 30 and Supplementary Fig. 31). In order to double-check these findings also fluorescence was used for NP detection. For this purpose we used CdSe/ZnS quantum dots (QDs, emission at 605 nm) with the organic fluorophore DY636 (Dyomics, emission at 657 nm) in the polymer shell with similar colloidal properties as the Au NPs. The QDs were administered to rats with the same protocol, and tissue slices of the liver were imaged with optical microscopy. Again, no NP signal (neither from the QD core nor from the fluorophore-labelled shell) could be detected above the autofluorescence background level (*cf.* Supplementary Fig. 33). While the low NP doses of 10^{13} - 10^{14} NPs per animal thus did not allow for observation of individual NPs in the liver slices used for TEM and fluorescence microscopy imaging, inductively coupled plasma mass spectrometry (ICP-MS) analyses performed on the entire liver had enough sensitivity for detecting the NPs and clearly demonstrated their present in the liver (*cf.* Supplementary Fig. 32 and Supplementary Fig. 35), confirming the data with radiolabelled NPs.

Knowing by detection of radiolabels (Figure 2a-d) and ICP-MS that the NPs in fact are dominantly retained in the liver, though at concentrations too low to allow for successful histology, we attempted to emulate *in vivo* behaviour of the liver by *in vitro* investigation on cell lines representing different cell types in the liver. We selected Kupffer cells, which are specialized stellate macrophages in the liver, and human umbilical vein endothelial cells (HUVECs). First, cellular uptake of polymer coated Au NPs and QDs was quantified in terms of intracellular Au and Cd/Se, respectively, as quantified by ICP-MS. NPs are incorporate by both cell types (Supplementary Fig. 36) and intracellular uptake of Au NPs and QDs is similar (*cf.* Figure 4a, b, and Supplementary Fig. 37). We attribute this to the similar surface chemistry of the

Au NPs and QDs, though time- and concentration-dependencies differ. Second, the intracellular location of the internalized Au NPs and QDs (with a fluorescence label in their polymer shell) was determined by confocal microscopy *via* colocalization with the lysosomal membrane marker LAMP-1 (*cf.* Supplementary Fig. 38). Data demonstrate time- and concentration dependent rise of localization of both types of NPs in the lysosomes of both, HUVECs (*cf.* Figure 4c, d, and Supplementary Fig. 39) and Kupffer cells (*cf.* Supplementary Fig. 40). Thus, our data indicate that NPs retained in the liver are localized in the lysosomes of macrophages and of epithelial cells. Due to their similar surface chemistry polymer-coated QDs show a similar behaviour as polymer-coated Au NPs.

Figure 4e shows that incubating polymer-coated QDs with a DY495 fluorescence label in their polymer shell with different proteolytic enzymes (trypsin, pronase, proteinase 3, and cathepsin G) leads to the degradation of the polymer shell, as visualized by the removal of the integrated fluorescent label from the QDs. Thus, presence of proteolytic enzymes leads to degradation of the polymer shell "in test tube". We hypothesized that proteolytic lysosomal enzymes present in endosomes and lysosomes may be responsible for the *in vitro* degradation of the polymer shell. HUVECs and Kupffer cells were incubated with polymer-coated QDs. Colocalization analysis of the fluorescence originating from the QD core and the fluorescence originating from the fluorescence of the DY495 label of the polymer shell indicate that after several hours the polymer shell label is partly displaced from the QD label, which is in agreement with findings of others[3]. In the medium the fluorescence of exocytosed QDs has a lower fraction of QD fluorescence compared to DY495 fluorescence, as it is found for QDs inside cells that have been analysed after cell lysis. Our data also directly show that intracellular enzymatic degradation of internalized QDs can cause partial removal of either the DY495-labeled polymer shell or the DY495 label, which are subsequently exocytosed as seen in Figure 4f.

The 24 h biodistribution of the polymer-coated ^{198}Au NPs from the present study (Figure 2b) is similar to that of 5 nm Au NPs coated with triphenylphosphine sulfonate (TPPS) in previous studies[22, 23] (Figure 5). Since the protein corona plays a significant role in the determination of the biokinetics of the intravenously injected Au NPs, the similar patterns indicate that the protein coronas seem to be very similar. For the virtually “naked” TPPS coated Au NPs it was shown that the coating was rather quickly removed in a cellular *in vitro* assay[24]. This is in agreement

with our findings in which the polymer coated Au NPs lose parts of their polymer coating *in vitro* as *in vivo*. Thus, in both cases the protein corona is formed on a partly "naked" surface of the Au NPs (*i.e.* a surface partially stripped off the original organic coating). This is the likely reason that leads to a similar biodistribution of TTPS and polymer coated NP.

Conclusions

Using radio-labelled Au cores and polymer shells, we show that the polymer shells of polymer-coated Au NPs are partially removed *in vitro* and *in vivo*. *In vivo*, NPs are mostly retained in the liver and fragments of the organic shell are excreted through the kidneys. *In vitro* experiments show that NPs internalized by HUVEC and Kupffer cells were localized in endosomal and lysosomal compartments. A partial separation of the organic shell from the inorganic core is caused by proteolytic enzymes present in these compartments. We believe *in vivo* degradation of the polymer shell is due to similar proteolytic digestion. Our findings indicate that the physicochemical properties and the integrity of NPs can change dramatically upon internalization by cells *in vitro* and *in vivo*. This may have potential consequences for drug targeting with NPs

Acknowledgements

This work was supported by Deutsche Forschungsgemeinschaft (DFG grant "PA794/11-1" to WJP, grant "SPP1313" to WGK) and the European Commission Seventh Framework Programme (EC-FP7 grant "ENPRA NMP4-SL-2009-228789" and "Neuronano NMP4-SL-2008-214547" to WGK). The authors would like to thank Nadine Senger, Sebastian Kaidel, Barbara Kupferschmid, and Barbara Krieger for technical assistance and to Dominik Hühn, Ron Gill, Markus Klapper, and Kenneth Dawson for helpful scientific discussions.

Author Contributions

WGK and WJP conceived the idea, designed and analysed the experiments, and mainly wrote the manuscript. All authors discussed the results, contributed to data analysis, and commented on the manuscript. AMA, ZA, JMM, TR, and IRdL prepared and characterized the nanoparticles. RH, KK, DJdA, and JR preformed the *in vitro* experiments. AW, NH, SH, and GKS carried out *in*

vivo experiments with radionucleotides. FA and RU carried out in vivo experiments with fluorescent nanoparticles. MG performed transmission electron microscopy measurements.

Additional information

Supplementary information accompanies this paper at www.nature.com/naturenanotechnology. Reprints and permission information is available online at http://npg.nature.com/reprintsandpermissions/. Correspondence and requests for materials should be addressed to WJP.

Materials and Methods

NP preparation and characterization: Au NPs (core diameter $d_c = 4.8 \pm 0.9$ nm, *cf.* Supplementary Fig. 1) were neutron activated, leading to conversion of parts of the Au atoms to the gamma-emitting isotope ^{198}Au[4]. The Au cores were coated by an amphiphilic polymer (poly(isobutylene–alt–maleic anhydride)–*graft*–dodecyl), to which the indium chelator 1,4,7,10-tetraazacyclododecane-1,4,7,10-tetraacetic acid (DOTA) had been integrated[5]. After addition of ^{111}In the resulting double-labelled NPs has a hydrodynamic diameter of $d_h = 13 \pm 1$ nm and a zeta-potential of -46 ± 16 mV (*cf.* Supplementary Fig. 14 and Fig. 15). The geometry of the NPs is shown in

Figure *1*. For details we refer to a previous publication[5]. CdSe/ZnS QDs (core diameter of $d_c = 4.7 \pm 1$ nm, *cf.* Supplementary Fig. 3) were synthesized according to standard protocol. The QDs were coated by the same amphiphilic polymer as the Au NPs, in which organic fluorophores were integrated. The QDs had a ζ-potential of -28 ± 4 mV (*cf.* Supplementary Fig. 20). For details we refer to a previous publication[5].

Animals: Healthy, female Wistar-Kyoto rats (WKY/Kyo@Rj rats, Janvier, Le Genest Saint Isle, France), 8–10 weeks of age (approximately 250 g body weight) were housed in pairs in humidity and temperature-controlled ventilated cages on a 12 h day/night cycle. Rodent diet and water were provided *ad libitum*. All experiments were conducted under German federal guidelines for

the use and care of laboratory animals and were approved by the Regierung von Oberbayern (Government of District of Upper Bavaria, Approval No. 55.2-1-54-2531-26-10) and by the Institutional Animal Care and Use Committee of the Helmholtz Center Munich.

NP administration and animal maintenance in metabolic cages: The entire administration has been already described previously[4, 19]. Briefly, the rats were anesthetized by inhalation of 5 % isoflurane until muscular tonus relaxed. NPs suspensions (50 to 70 µL containing 1-10 µg of double-labelled gold NPs) were administered to the animals via intravenous injection into the tail vein of the animal. After administration of the NPs suspensions, rats were kept individually in metabolic cages for separate collection of total urine and feces.

Sample preparation and radio analysis: One hour or 24 hours post injection, rats were anesthetized and euthanized by exsanguination via the abdominal aorta. Radio analysis was performed on four rats for each time point according to previously published protocols[4, 23]. Briefly, total organs, tissues, body fluids, the remaining carcass, and total urinary and faecal excretions were sampled and analysed γ-spectrometrically[4, 19]. The ^{198}Au or ^{111}In radioactivities of all samples were measured without any further sample preparation by γ-spectroscopy. Small organ and tissue samples were analysed in a lead-shielded, 10 mL well type NaI(Tl) scintillation detector, while a lead-shielded, 1 L well type NaI(Tl) scintillation detector was used for large samples like the remaining carcass. Compton correction was carried out using the gamma acquisition analysis software Genie 2000 (Canberra Industries, Rüsselsheim, Germany). Count rates were adjusted for physical decay and background radiation. Additionally, the ^{198}Au or ^{111}In count rates were calibrated to either a ^{198}Au or ^{111}In reference source at a reference date in order to correlate ^{198}Au and ^{111}In radioactivities to the numbers and masses of the Au NPs. Samples yielding net counts (*i.e.* background-corrected counts) in the photo-peak region-of-interest of either the ^{198}Au or the ^{111}In γ-spectrum were defined to be below the detection limit when they were less than three standard deviations of the background counts of this region-of-interest. While dissecting, no organs were cut and all fluids were cannulated when necessary in order to avoid cross contamination. We quantitatively determined the entire ^{198}Au and ^{111}In dose independently from each other in the entire animal by analysing for each radio-isotope each organ and tissue and total excretion. Thus, for each radio-isotope a 100 % balance of the biodistribution was performed.

Blood correction: Blood contents of organs and the remaining body were calculated according to the findings of Oeff *et* al.[20] as described previously[22, 23].

Calculations and statistical analysis: All calculated data are given as a percentage of the relevant integral radioactivity of all samples in each animal with the standard error of the mean (SEM) for both radio-isotopes.

Accompanying "in test tube" and *in vitro* experiments with QDs: In order to support the *in vivo* observations as obtained with polymer-coated Au NPs with double radionucleotide labelling additional "in test tube" and *in vitro* experiments were performed with polymer-coated QDs with double fluorescence labelling (one colour for the inorganic NP core, one colour for the organic polymer shell) which had similar geometry, surface chemistry, and colloidal properties. "In test tube" polymer coated QDs were incubated with different proteolytic enzymes and resulting fragments of the DY495-labelled polymer shell / released DY495 were separated from the NPs by filtration. The amount of released fluorescence label from the polymer coating was quantified with fluorescence spectroscopy. For *in vitro* experiments HUVECs and Kupffer cells (which are relevant for NPs present in the liver) were exposed to polymer coated QDs-labelled with different fluorophore labels in their polymer shell. Colocalization experiments between the QD core and the polymer shell label were performed. The fluorescence spectra of exocytosed QDs and QDs found in cell lysate were compared (*cf.* Supplementary Fig. 46 - Supplementary Fig. 49).

Figures

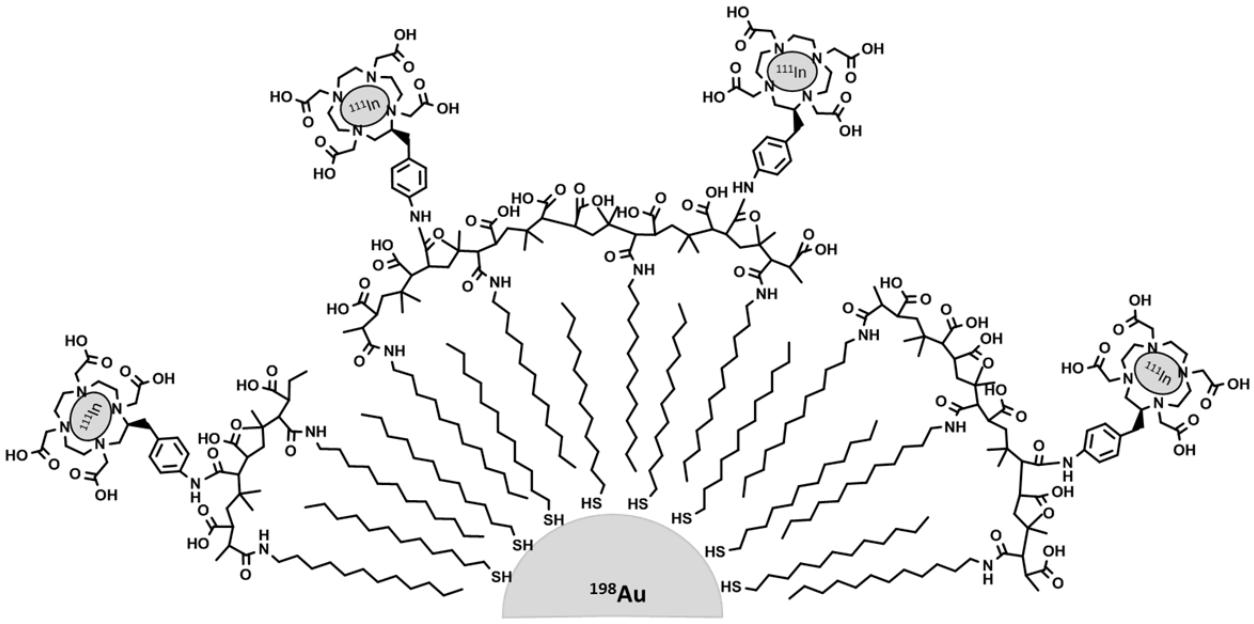

Figure 1: *Sketch of the NPs with double radio-label. Au cores were synthesised in organic phase by reduction of* Au^{3+} *and the resulting NPs were stabilized by a ligand shell of dodecanethiol. Upon neutron activation, some of the Au atoms were converted into the radioactive isotope* ^{198}*Au, which forms the radiolabelled core. A shell of the amphiphilic polymer poly(isobutylene–alt–maleic anhydride)–graft–dodecyl was then wrapped around the Au core and rendered the NP water-soluble. DOTA was integrated into the polymer shell and was loaded with In (enriched with the radioactive isotope* ^{111}*In, which acted as the shell label). In this way NP core and shell are individually labelled by* ^{198}*Au and* ^{111}*In, respectively.*

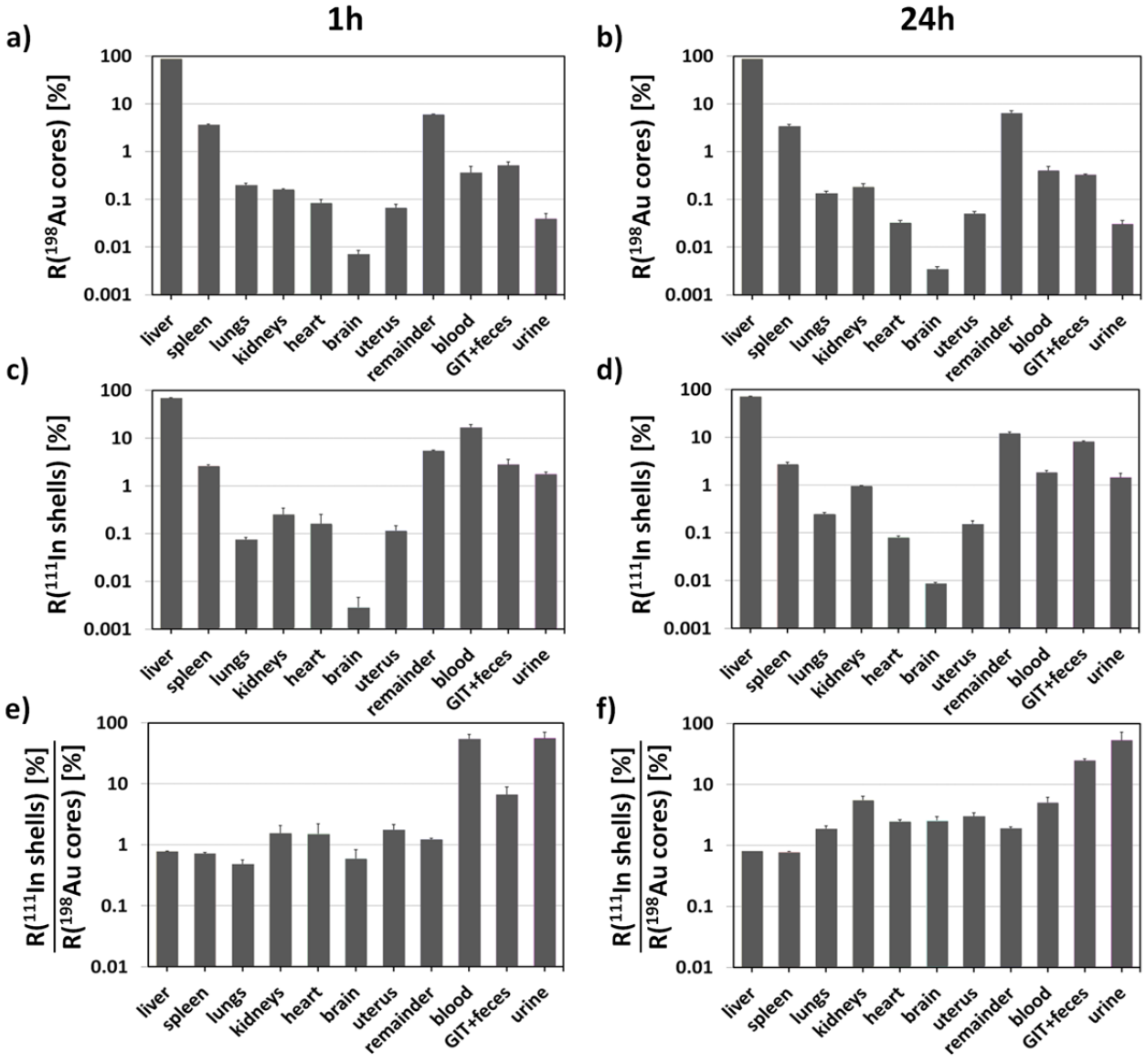

Figure 2: *Biodistribution of double-labelled NPs. Au NPs (with core diameter d_c = 4.8 ± 0.9 nm) with an ^{198}Au core radiolabel and an ^{111}In shell radiolabel had been intravenously injected into the tail vein of Wistar-Kyoto rats and their radioactivities were determined in different organs. Graphs show the quantitative balance (i.e. the sum of all* ^{198}Au or ^{111}In *radioactivities over all organs and tissues, the remaining carcass, and total faecal and urinary excretion is 100 %) of the 1 h and 24 h biodistribution of double-labelled Au NPs. The retentions R, given as mean data (±SEM) are denoted in percent of the total radioactivity for the respective radio-isotope (n = 4 animals per data point). "Remainder" represents radiolabels found in the remaining rest of the carcass after sampling of organs, i.e. soft tissues, skin and skeleton, etc. "GIT+feces" represents the radiolabels found in the gastro-intestinal-tract and in feces (note that after 1 hour no radiolabels were found in feces). "Blood" represents the total content of radiolabels as calculated from the measured content in the blood sample and the estimate of the total blood volume, cf. Methods. a, b) biodistribution of the ^{198}Au NP core radiolabel. c, d) biodistribution of*

the ^{111}In shell radiolabel. e, f) ratio of ^{111}In shell to ^{198}Au NP radiolabel in each organ and tissue. The data show that more ^{111}In shell labels than ^{198}Au core labels were detected in blood, urine, and GIT and feces at any time point. Data are also plotted in linear scale in Supplementary Fig. 25, and enlisted in Supplementary Table 1 and Supplementary Table 2.

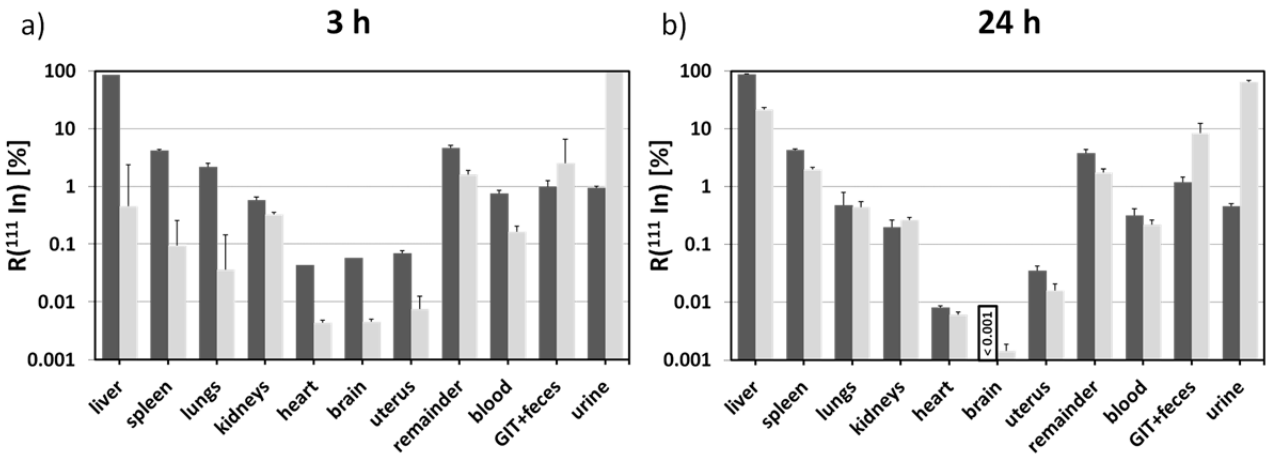

Figure 3: *Quantitative biodistribution of soluble free ^{111}In ions and ^{111}In-DPTA complexes. C57BL/6 mice were intravenously injected with free ^{111}In ions and chelated ^{111}In in the form of ^{111}In-DPTA complexes. Biodistribution was monitored at 3 h (a) and 24 h (b) by measuring the radioactivities of the different organs. The graph shows the percent retention R of ^{111}In for free (dark grey bars) and chelated (light grey bars) ^{111}In in whole organs and tissues, the remaining carcass without sampled organs, the gastro-intestinal-tract and the total feces "GIT+feces", and urinary excretion. The retentions R are given as mean data (±SEM) and are denoted in percent of the total radioactivity for the respective radio-isotope (n = 4 animals per data point). Data demonstrate that the biodistribution of ^{111}In ions and of ^{111}In-DPTA chelate complexes is different, in particular in liver and urine.*

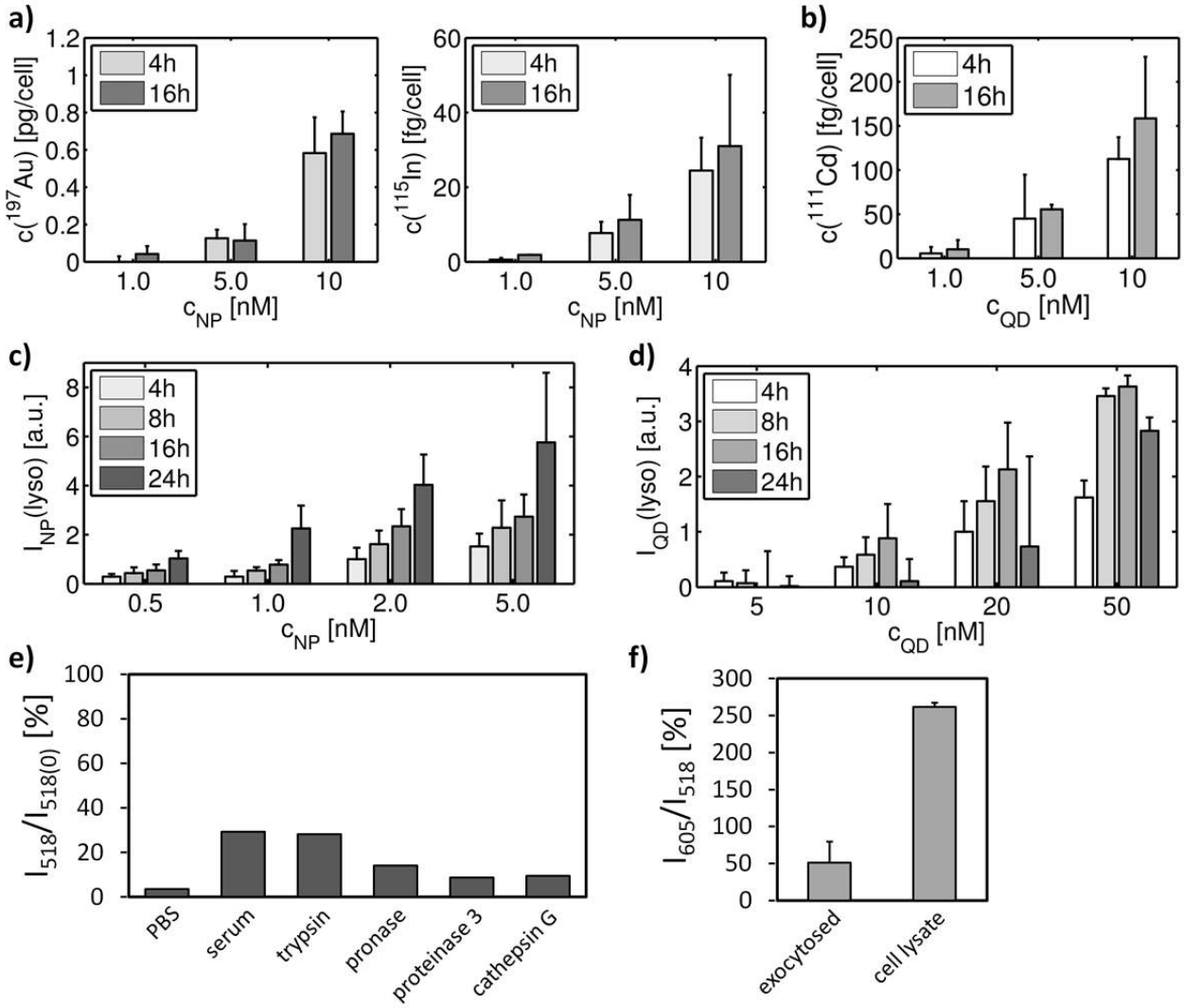

Figure 4: *Cellular internalization and degradation of polymer coated Au NPs and QDs by proteases "in test tube" and in vitro. a, b) ICP-MS analysis of the uptake of (a) Au NPs with In in their polymer shell and (b) polymer-coated CdSe/ZnS QDs by HUVECs. Shown is the content (a: Au, In; b: Cd) per cell after indicated incubation times with different NP concentrations of c_{NP} = 1, 5 and 10 nM. c, d) Lysosomal enrichment of (c) fluorescence-labelled Au NPs and (d) CdSe/Zn QDs in HUVECs. The fluorescence intensity I(lyso) originating from the NPs is given for different NP concentrations c_{NP}. e) Ratio $I_{518}/I_{518(0)}$ of fluorescence intensity of DY495 label released from the shell around the QDs after 24 h "in test tube" incubation with phosphate buffered saline (PBS, pH = 7.4), in the presence of 10 % fetal bovine serum (serum), trypsin (0.05 %), pronase (0.2 units/mL), proteinase 3 (0.003 units/mL), and cathepsin G (13 units/mL). The ratio $I_{518}/I_{518(0)}$ was quantified by measuring the fluorescence I_{518} of DY495 (@ 518 nm) of the released DY495 label after separation from the QD core by ultrafiltration, as compared to the original fluorescence $I_{518(0)}$ of the DY495 label attached to the QDs. f) Ratio of QD and DY495 fluorescence intensities (I_{605}/I_{518}) for exocytosed QDs and QDs found inside Kupffer cells (cell lysate). Kupffer cells were incubated with the QDs for 22 h followed by additional 3 h*

incubation after removing the free QDs from the medium. All data are given as mean values ± standard deviation. Data demonstrate partial removal of the polymer shell from the NP cores in vitro.

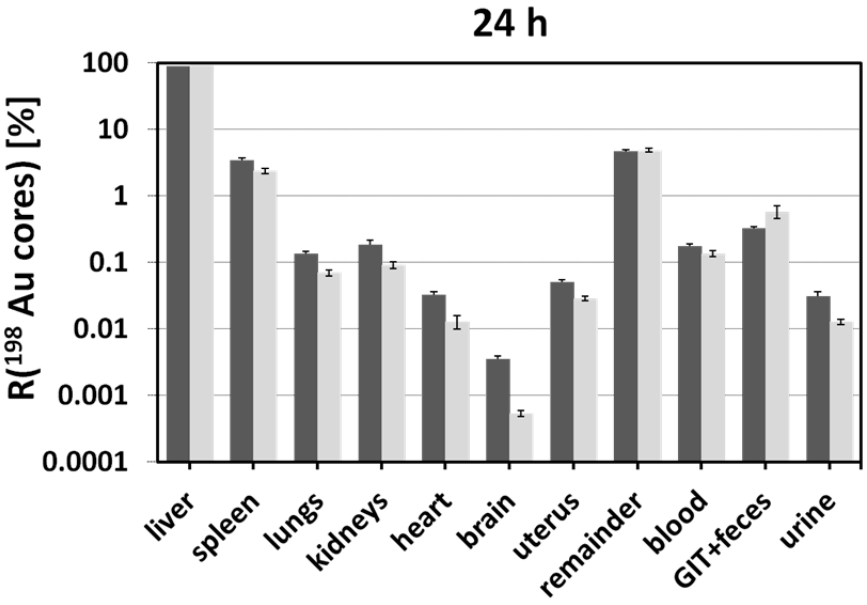

Figure 5*: Quantitative 24 h biodistribution of i.v. injected, monodisperse Au NPs (d_c = 5 nm) coated with triphenylphosphine (TPPS) (dark grey bars; data taken from our previous study [22]) and of Au NPs (d_c = 4.8 ± 0.9 nm) coated with a DOTA-modified polymer shell (light grey bars; data taken from Figure 2b) in Wistar-Kyoto rats. For each time point data for the retention R of the ^{198}Au cores are given in percent (mean ± SEM; n = 4 animals) of the total radioactivity of each entire animal. Data demonstrate that the biodistribution of the Au NPs with the two different surface coatings (TPPS versus polymer coating) is similar.*

References:

1. Rivera Gil, P. et al. The challenge to relate the physicochemical properties of colloidal nanoparticles to their cytotoxicity. *Acc. Chem. Res.* **46**, 743-749 (2013).
2. Chanana, M., Rivera Gil, P., Correa-Duarte, M. A., Parak, W. J. & Liz-Marzán, L. M. Physicochemical properties of protein-coated gold nanoparticles in biological fluids and cells before and after proteolytic digestion. *Angew. Chem., Int. Ed.* **52**, 4179-4183 (2013).
3. Chen, H. W., Zou, P., Connarn, J., Paholak, H. & Sun, D. X. Intracellular dissociation of a polymer coating from nanoparticles. *Nano Research* **5**, 815-825 (2012).
4. Semmler-Behnke, M. et al. Biodistribution of 1.4- and 18-nm gold particles in rats. *Small* **4**, 2108-2111 (2008).
5. Ali, Z. et al. Multifunctional nanoparticles for dual imaging. *Anal. Chem.* **83**, 2877-2882 (2011).
6. Kreyling, W. G. et al. Interspecies comparison of phagolysosomal pH in alveolar macrophages. *Inhalation Toxicol.* **3**, 91-100 (1991).
7. Soenen, S. J. H. et al. Intracellular nanoparticle coating stability determines nanoparticle diagnostics efficacy and cell functionality. *Small* **6**, 2136-2145 (2010).
8. Levy, M. et al. Long term *in vivo* biotransformation of iron oxide nanoparticles. *Biomaterials* **32**, 3988-3999 (2011).
9. Derfus, A. M., Chan, W. C. W. & Bhatia, S. N. Probing the cytotoxicity of semiconductor quantum dots. *Nano Lett.* **4**, 11-18 (2004).
10. Kirchner, C. et al. Cytotoxicity of colloidal CdSe and CdSe/ZnS nanoparticles. *Nano Lett.* **5**, 331-338 (2005).
11. Kittler, S., Greulich, C., Diendorf, J., Koller, M. & Epple, M. Toxicity of silver nanoparticles increases during storage because of slow dissolution under release of silver ions. *Chem. Mater.* **22**, 4548-4554 (2010).
12. Caballero-Díaz, E. et al. The toxicity of silver nanoparticles depends on their uptake by cells and thus on their surface chemistry. *Part. Part. Syst. Charact.* **30**, 1079-1085 (2013).
13. Bose, K., Koch, M., Cavelius, C., Kiemer, A. K. & Kraegeloh, A. A correlative analysis of gold nanoparticles internalized by A549 cells. *Part. Part. Syst. Charact.* **31**, 439-448 (2014).
14. Lunov, O. et al. Lysosomal degradation of the carboxydextran shell of coated superparamagnetic iron oxide nanoparticles and the fate of professional phagocytes. *Biomaterials* **31**, 9015-9022 (2010).
15. Tietze, R. et al. Efficient drug-delivery using magnetic nanoparticles - biodistribution and therapeutic effects in tumour bearing rabbits. *Nanomed.-Nanotechnol.* **9**, 961-971 (2013).
16. Ducongé, F. et al. Fluorine-18-labeled phospholipid quantum dot micelles for *in vivo* multimodal imaging from whole body to cellular scales. *Bioconjugate Chem.* **19**, 1921-1926 (2008).
17. Sée, V. et al. Cathepsin l digestion of nanobioconjugates upon endocytosis. *ACS Nano* **3**, 2461-2468 (2009).

18. Wang, F. et al. The biomolecular corona is retained during nanoparticle uptake and protects the cells from the damage induced by cationic nanoparticles until degraded in the lysosomes. *Nanomed.-Nanotechnol.* **9**, 1159-1168 (2013).

19. Schleh, C. et al. Size and surface charge of gold nanoparticles determine absorption across intestinal barriers and accumulation in secondary target organs after oral administration. *Nanotoxicology* **6**, 36-46 (2012).

20. Oeff, K., Krentz, K. & Kessel, M. J-131-Clearance der normalen und pathologischen Magenschleimhaut. *Klin. Wochenschr.* **33**, 59-63 (1955).

21. Kreyling, W. G. et al. Air-blood barrier translocation of tracheally instilled gold nanoparticles inversely depends on particle size. *ACS Nano* **8**, 222-233 (2014).

22. Lipka, M. et al. Biodistribution of peg-modified gold nanoparticles following intratracheal instillation and intravenous injection. *Biomaterials* **31**, 6574-6581 (2010).

23. Hirn, S. et al. Particle size-dependent and surface charge-dependent biodistribution of gold nanoparticles after intravenous administration. *Eur. J. Pharm. Biopharm.* **77**, 407-416 (2011).

24. Pan, Y. et al. Gold nanoparticles of diameter 1.4 nm trigger necrosis by oxidative stress and mitochondrial damage. *Small* **5**, 2067-2076 (2009).

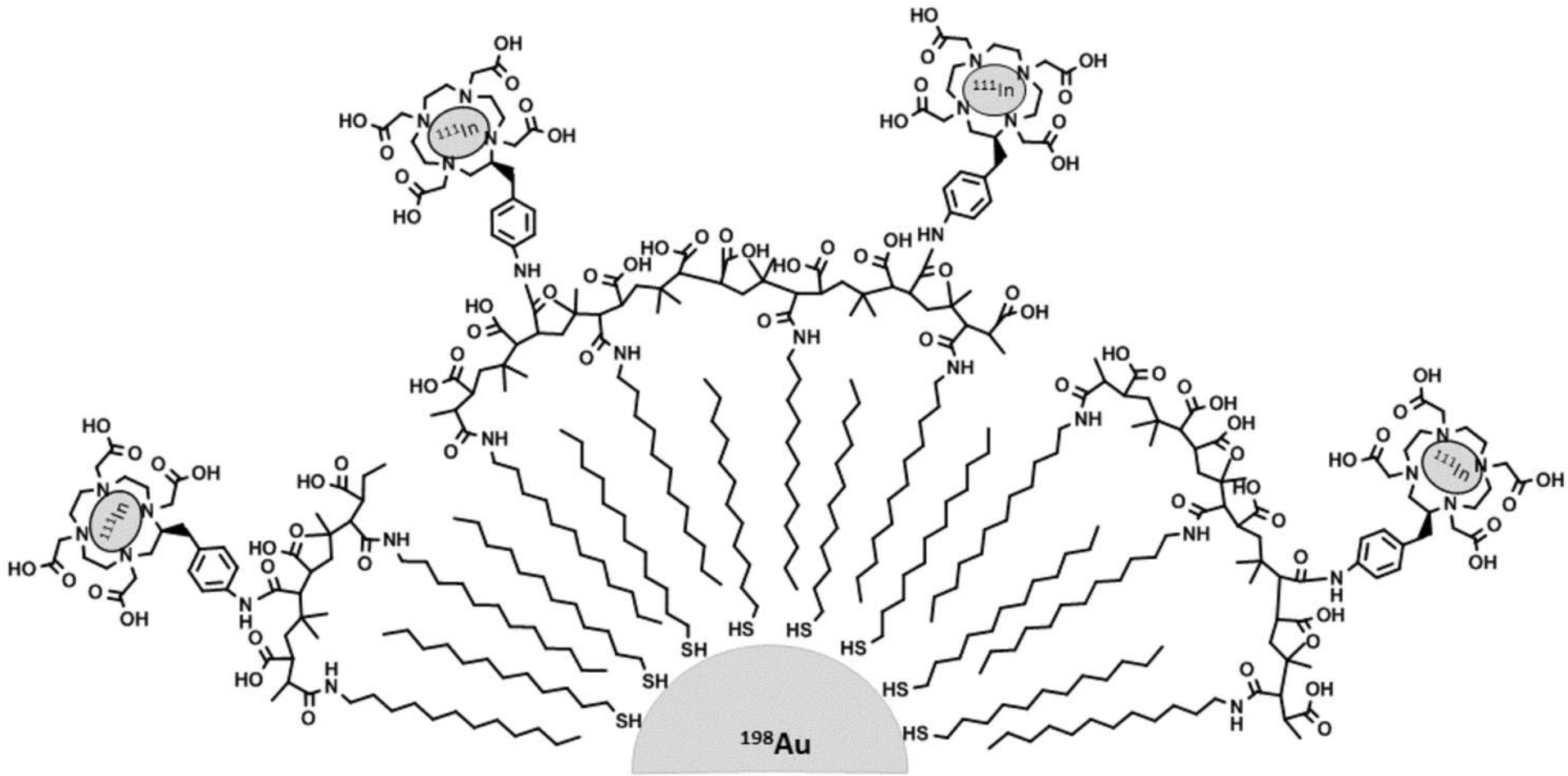
^{111}In
^{198}Au

a)

1h

b)

24h

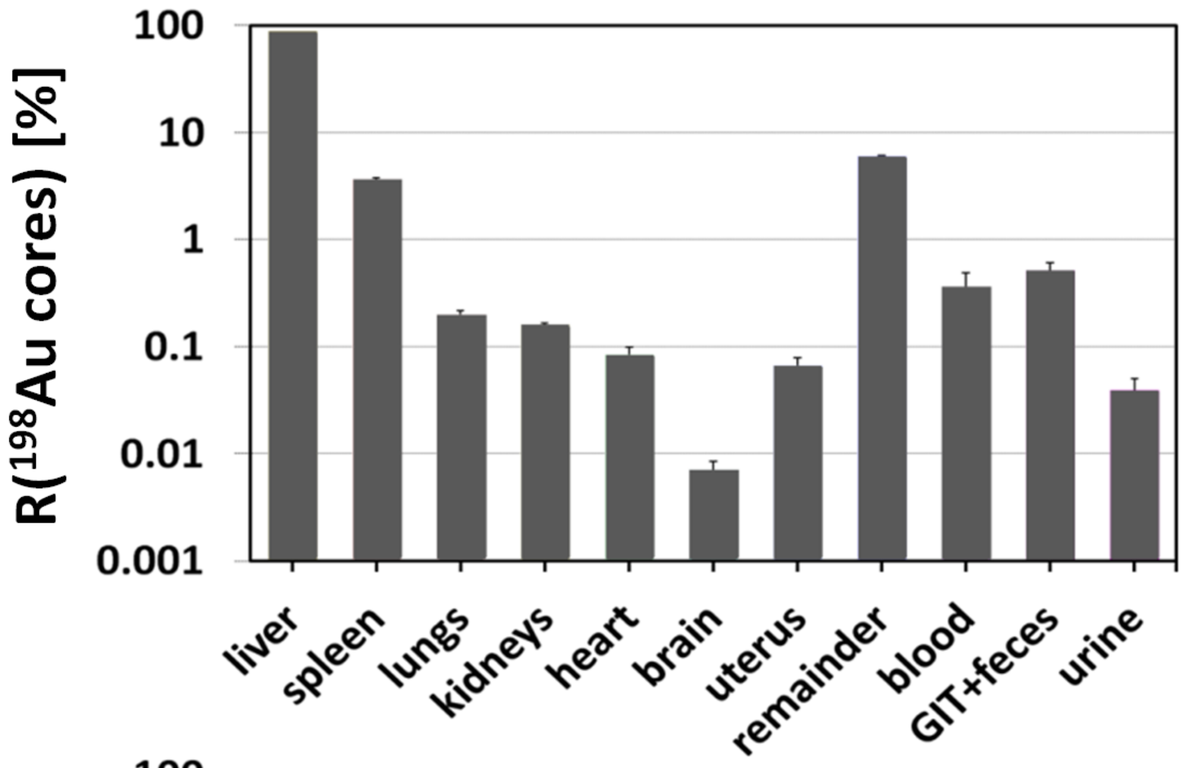

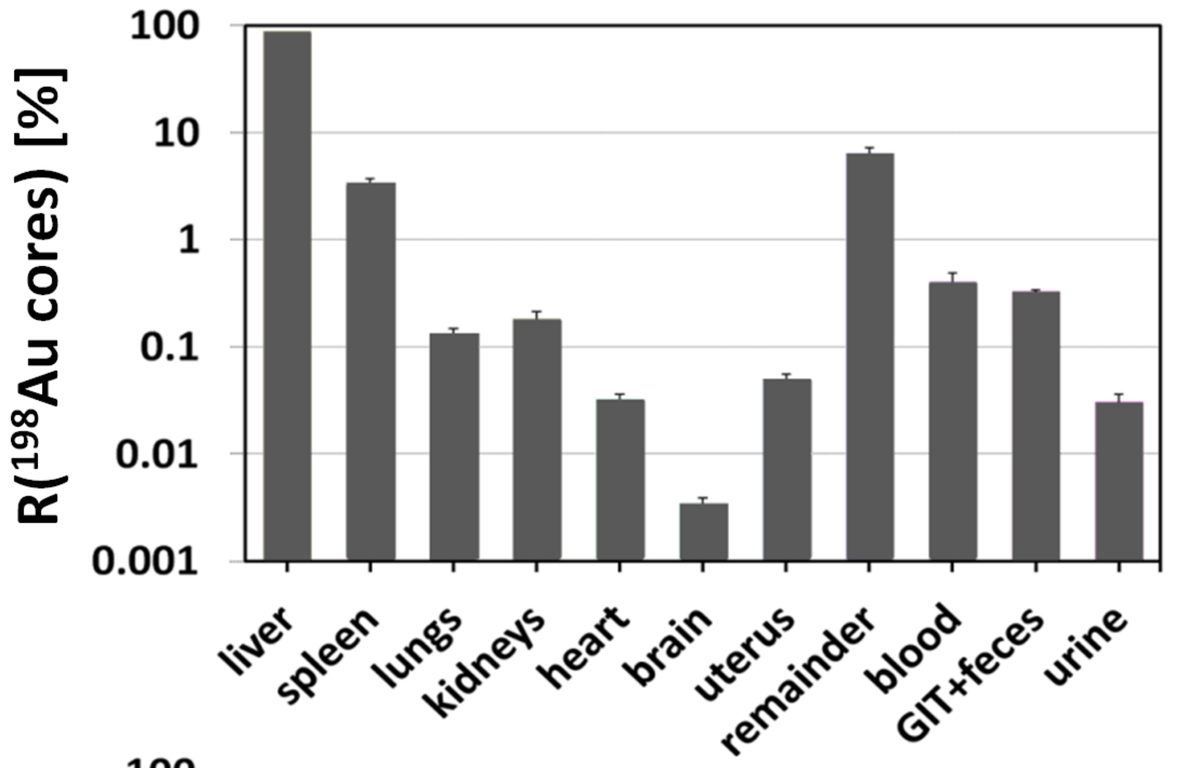

c)

d)

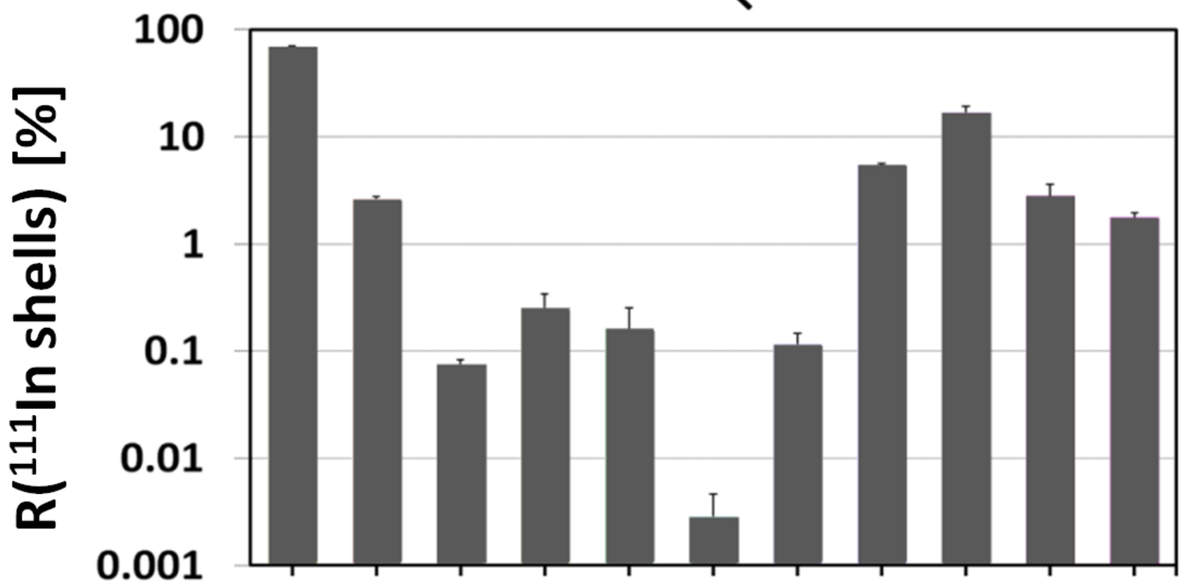

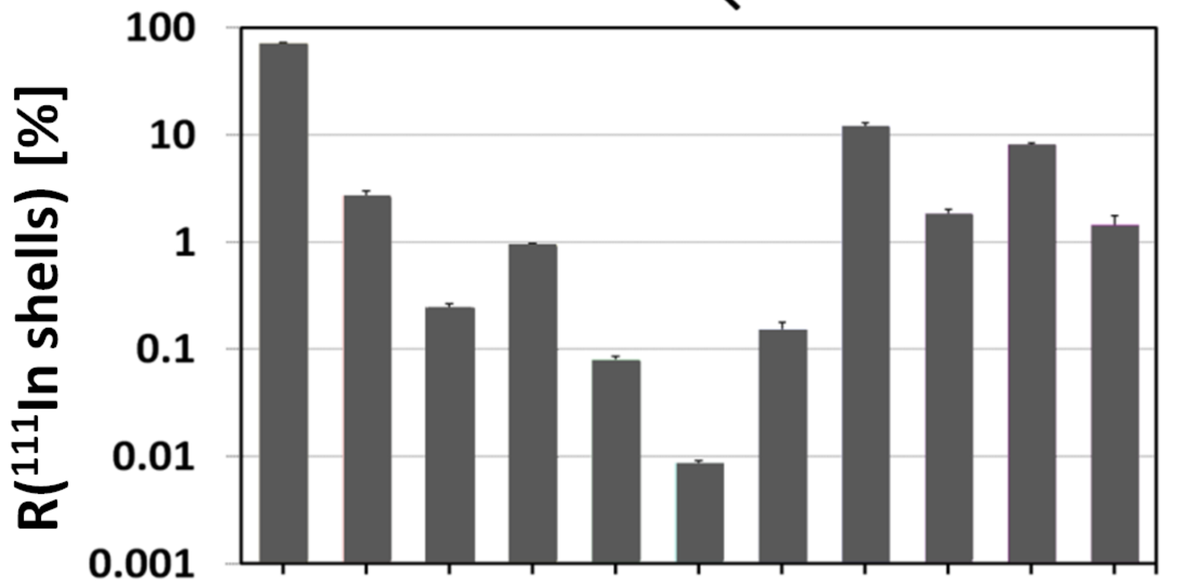

e)

f)

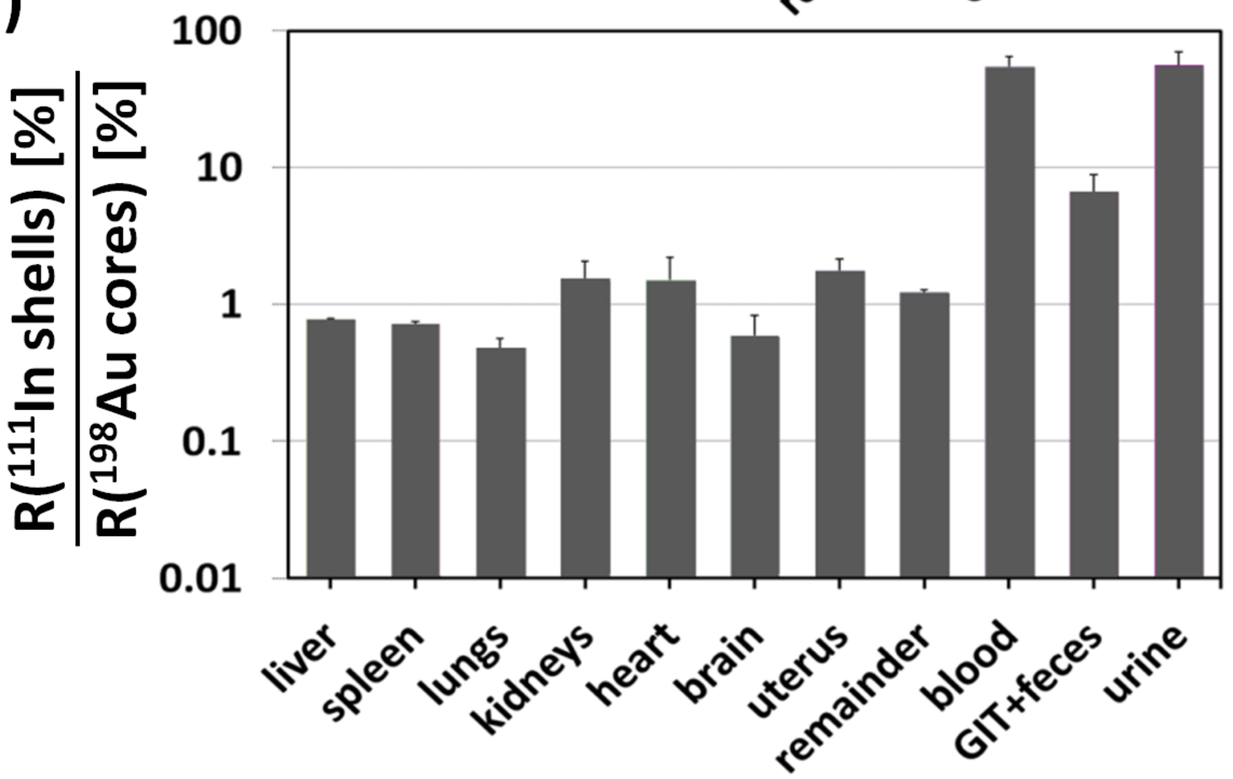

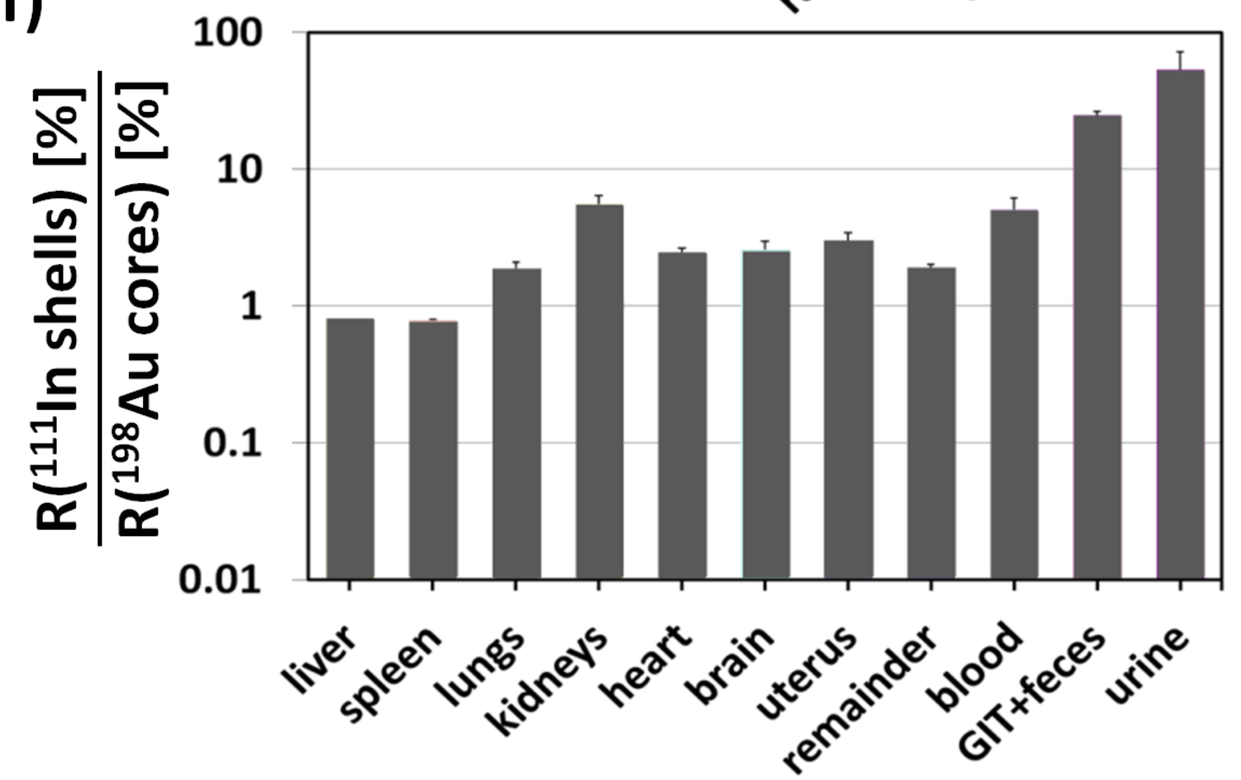

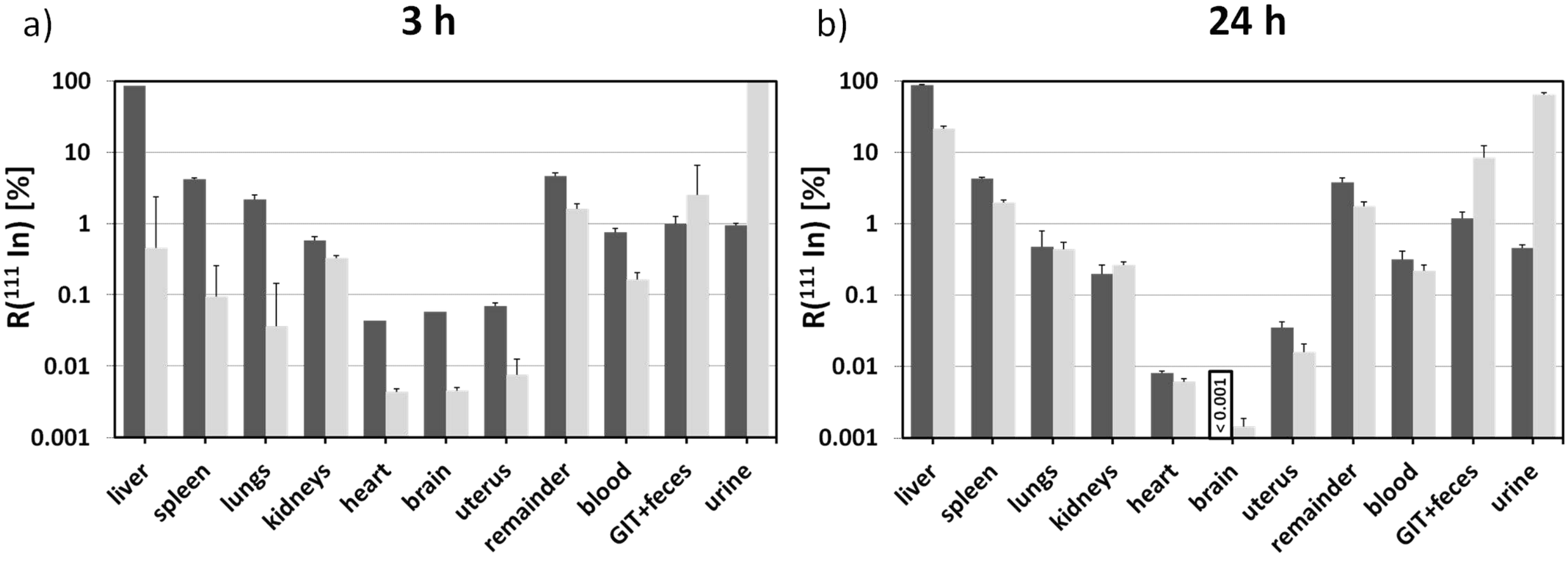
a)
3 h
b)
24 h
R(111 In) [%]
100
10
1
0.1
0.01
0.001
< 0.001
liver
spleen
lungs
kidneys
heart
brain
uterus
remainder
blood
GIT+feces
urine

a)

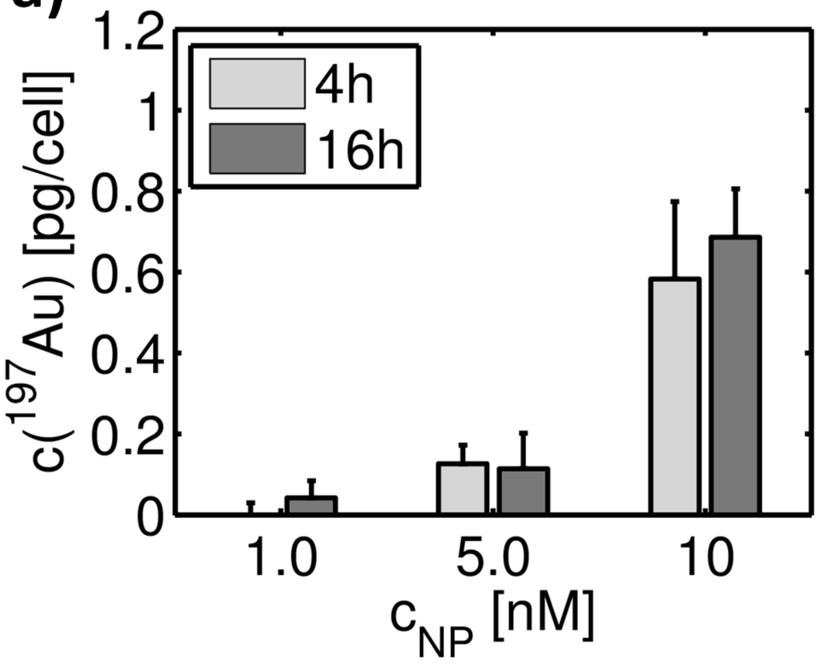
4h
16h
c(197Au) [pg/cell]
1.2
1
0.8
0.6
0.4
0.2
0
1.0
5.0
10
cNP [nM]

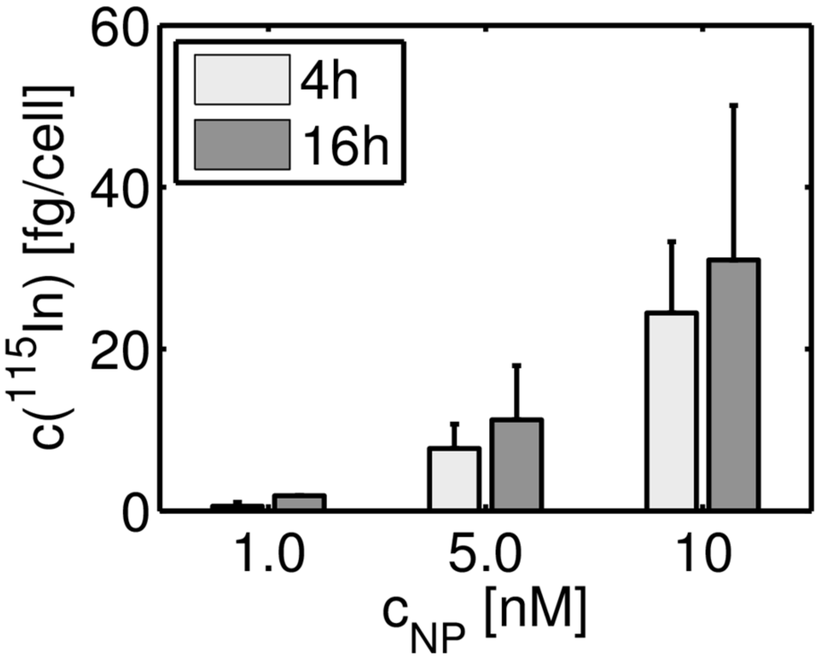
4h
16h
c(115In) [fg/cell]
60
40
20
0
1.0
5.0
10
cNP [nM]

b)

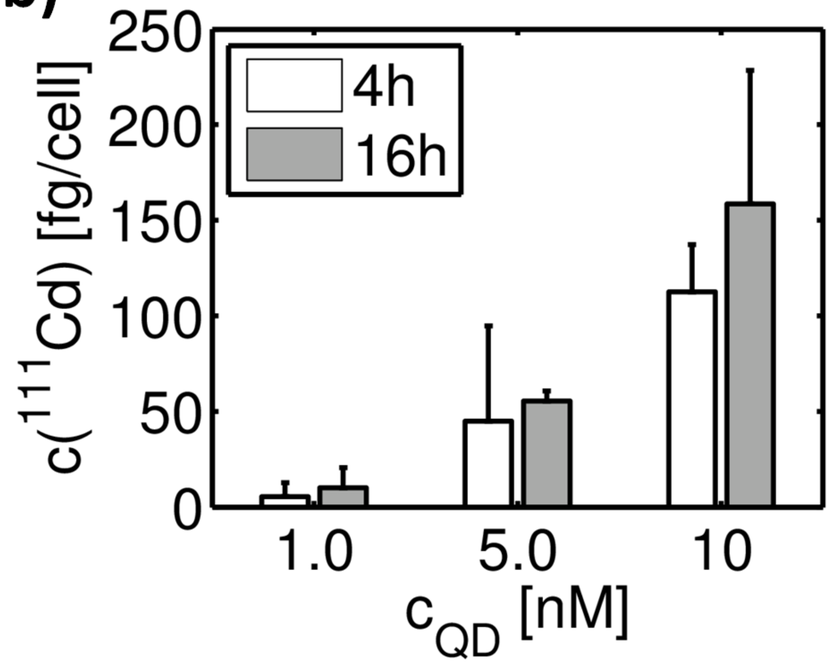
4h
16h
c(111Cd) [fg/cell]
250
200
150
100
50
0
1.0
5.0
10
cQD [nM]

c)

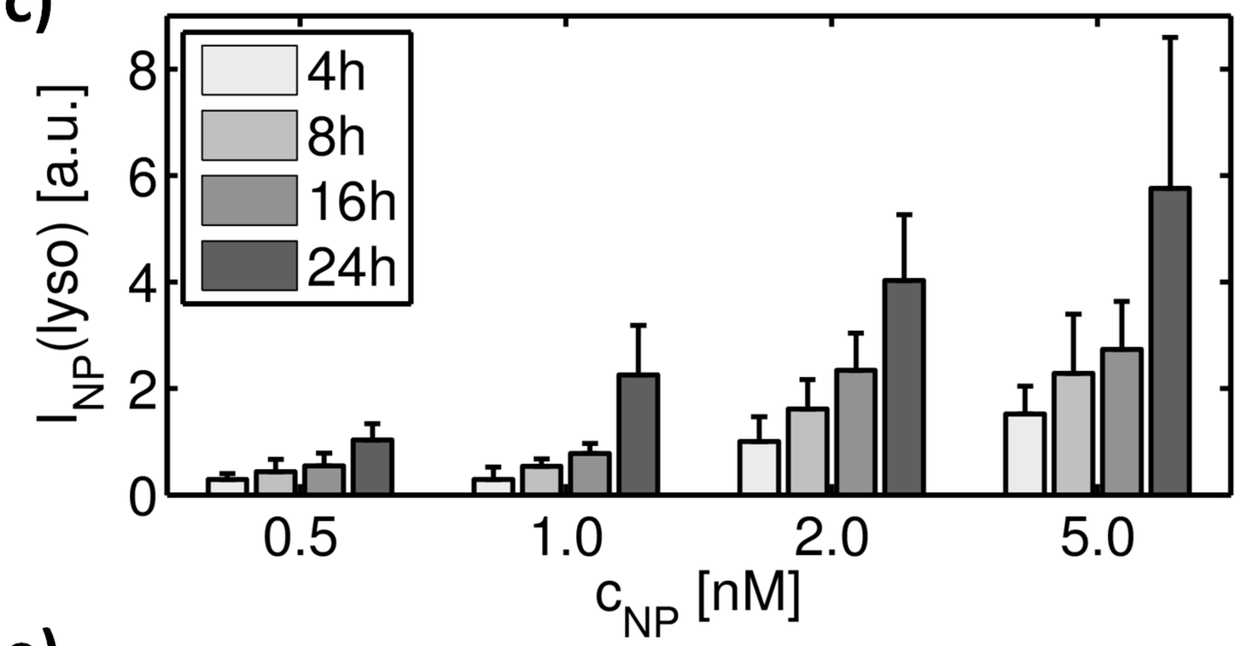
4h
8h
16h
24h
INP(lyso) [a.u.]
8
6
4
2
0
0.5
1.0
2.0
5.0
cNP [nM]

d)

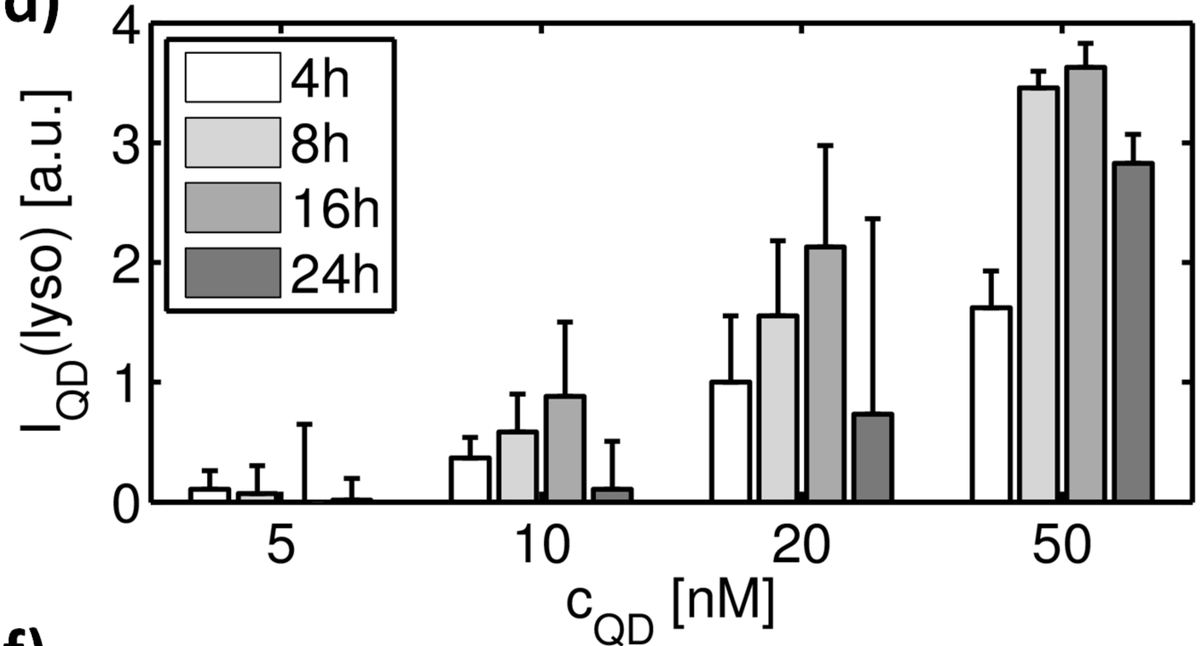
4h
8h
16h
24h
IQD(lyso) [a.u.]
4
3
2
1
0
5
10
20
50
cQD [nM]

e)

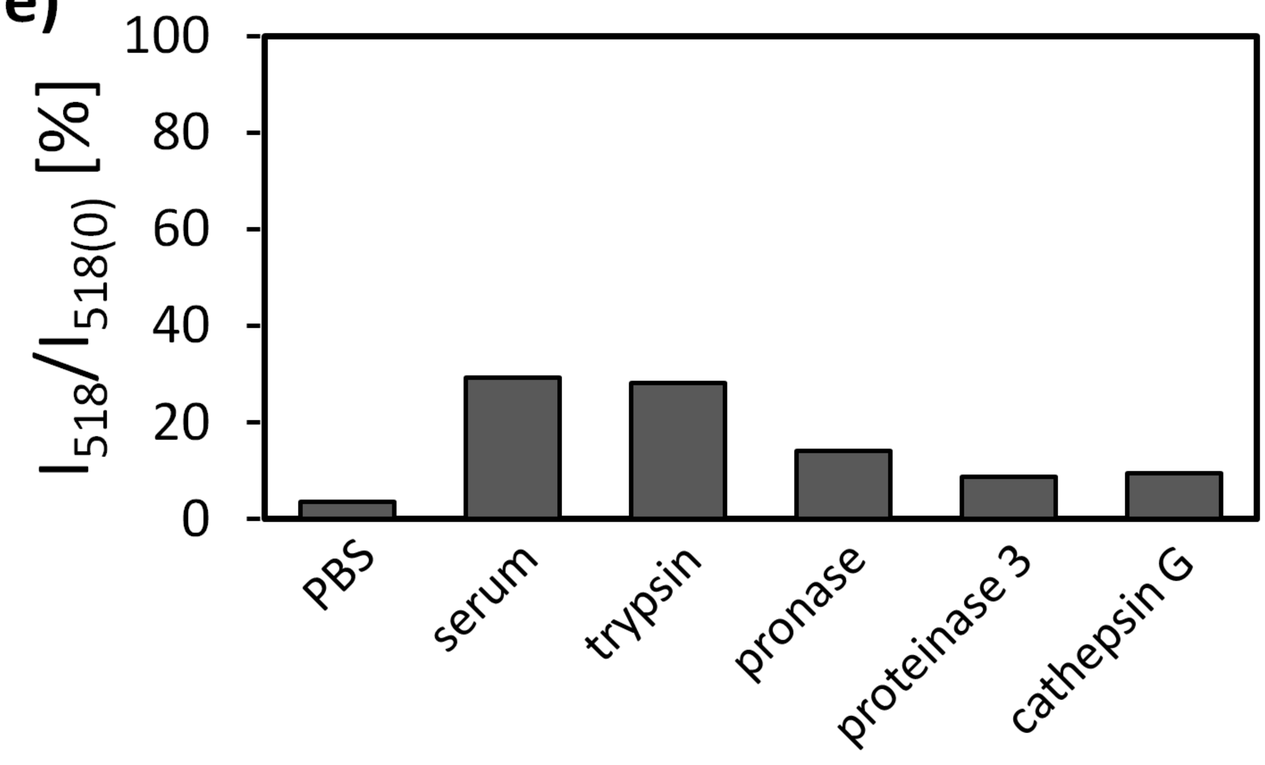
I518/I518(0) [%]
100
80
60
40
20
0
PBS
serum
trypsin
pronase
proteinase 3
cathepsin G

f)

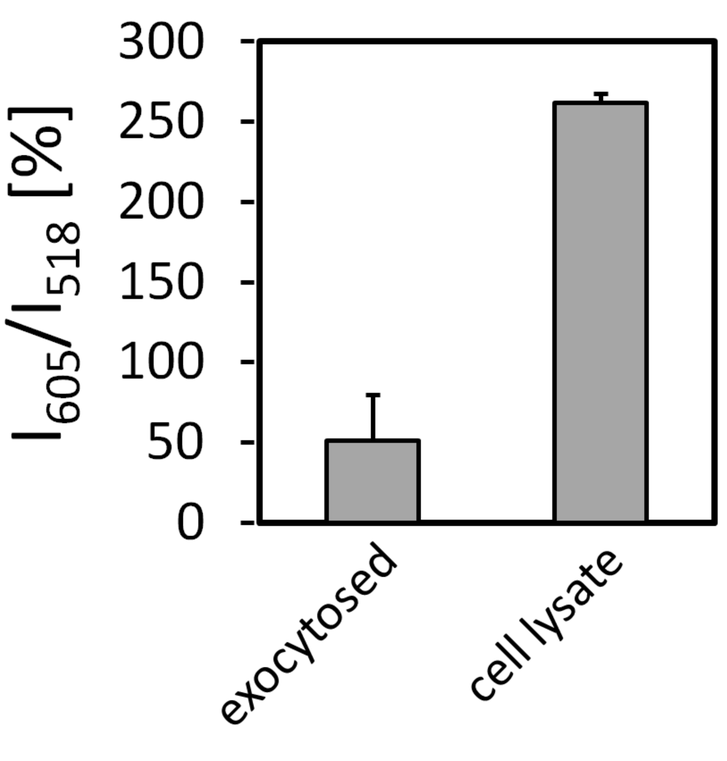
I605/I518 [%]
300
250
200
150
100
50
0
exocytosed
cell lysate

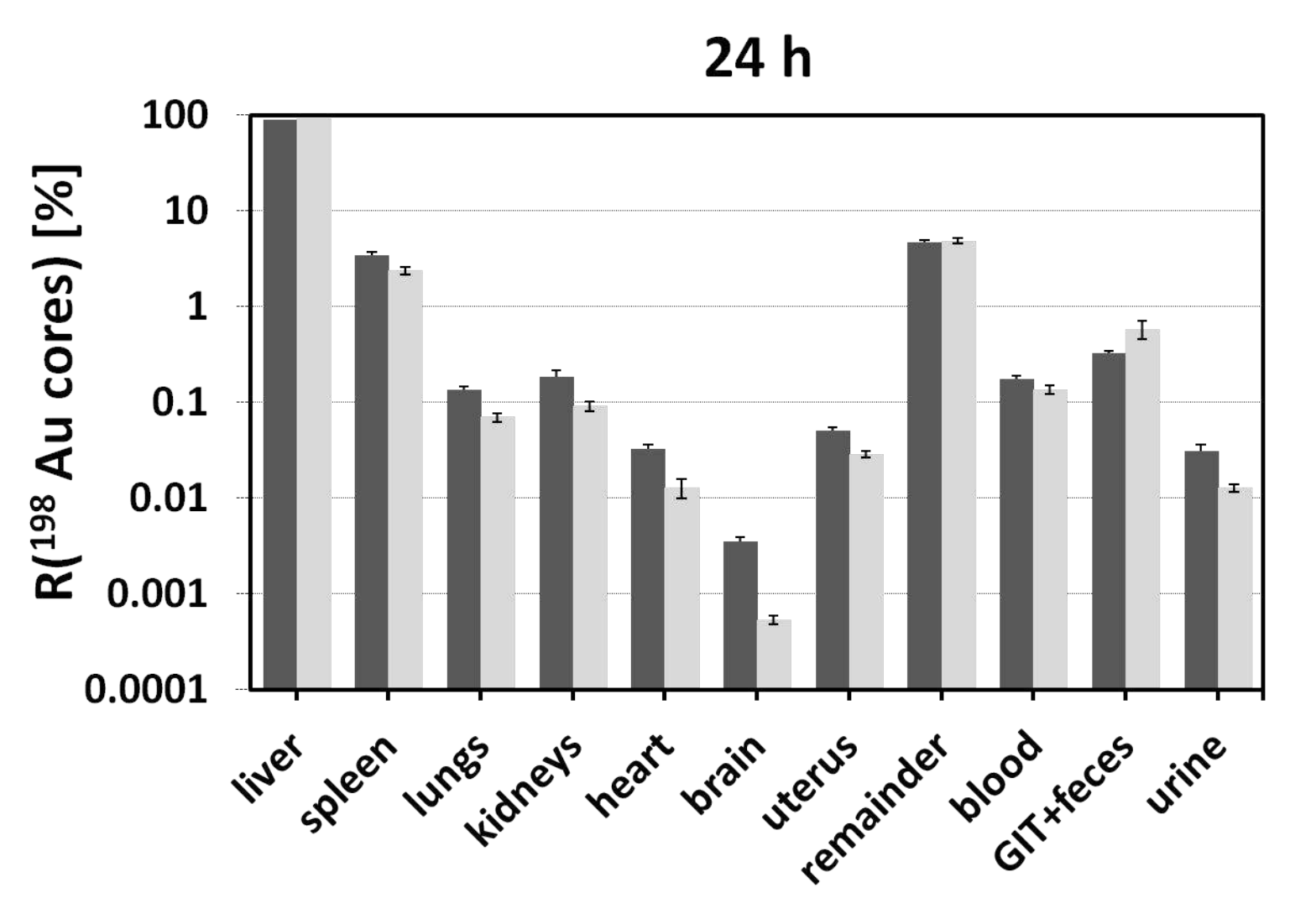
24 h
R(198 Au cores) [%]
100
10
1
0.1
0.01
0.001
0.0001
liver
spleen
lungs
kidneys
heart
brain
uterus
remainder
blood
GIT+feces
urine